A constant-head well permeameter method for measuring field-saturated hydraulic conductivity above an impermeable layer

Masaki Hayashi[1] and William L. Quinton[2]

[1]*Department of Geology and Geophysics, University of Calgary, Calgary, Alberta, Canada T2N 1N4 (e-mail: hayashi@ucalgary.ca); and* [2]*Department of Geography, Simon Fraser University, Burnaby, British Columbia, Canada V2X 9S6.* *Received 9 September 2003, accepted 17 February 2004.*

Hayashi, M. and Quinton, W. L. 2004. **A constant-head well permeameter method for measuring field-saturated hydraulic conductivity above an impermeable layer**. Can. J. Soil Sci. **84**: 255–264. Hydrologic understanding of mountainous and northern regions of Canada is poor owing to the lack of critical field data such as hydraulic conductivity. A portable field instrument, the Guelph permeameter (GP), is a promising tool for measuring field-saturated hydraulic conductivity in remote watersheds inaccessible by motorized vehicles. In order to extend the applicability of the GP method to relatively thin soils underlain by impermeable bedrock or permafrost, a new set of shape factors was determined by numerical simulation. The new shape factors gave accurate values of field-saturated hydraulic conductivity when tested in the laboratory. The impermeable layer causes flow around the auger hole to be primarily horizontal. Therefore, the GP method measures a predominantly horizontal field-saturated hydraulic conductivity in these thin soils. The measured conductivity represents a weighted average of the soil surrounding the submerged surface of the auger hole. In layered soil, the weight is greater for the layers close to the bottom of the hole than for those close to the top.

Key words: Guelph permeameter, hydraulic conductivity, forest hydrology, permafrost, peat

Hayashi, M. et Quinton, W. L. 2004. **Détermination de la conductivité hydraulique des terrains saturés surmontant une couche imperméable au moyen d'un perméamètre à tête de forage stable**. Can. J. Soil Sci. **84**: 255–264. On comprend mal l'hydrologie des régions montagneuses et nordiques du Canada à cause du manque de données indispensables sur la conductivité hydraulique prélevées sur le terrain. Le perméamètre Guelph (PG), un appareil portatif, promet beaucoup pour mesurer la conductivité hydraulique des terrains saturés dans les bassins hydrographiques reculés, inaccessibles par véhicule motorisé. Pour étendre l'usage du PG aux sols relativement minces couvrant une assise rocheuse imperméable ou le permagel, les auteurs ont conçu un nouveau jeu de paramètres de forme par simulation numérique. Ces paramètres ont donné une valeur précise de la conductivité hydraulique pour les terrains saturés lors des essais en laboratoire. La couche imperméable permet une circulation principalement horizontale autour du trou de forage. L'appareil mesure donc la conductivité hydraulique d'un flux essentiellement horizontal au point de saturation dans ces sols minces. La conductivité obtenue constitue une moyenne pondérée du sol qui entoure la surface submergée de la sonde. Pour la succession de couches, le poids est plus grand dans les strates près du fond que dans celles en surface.

Mots clés: Perméamètre Guelph, conductivité hydraulique, hydrologie forestière, permagel, sphaigne

The influence of anthropogenic activities, such as agriculture and forestry, on water resources has been the subject of numerous hydrological studies in Canada and elsewhere. Hydrological models are frequently used to evaluate the response of watersheds to changes in land cover and climate. The hydraulic conductivity of the near-surface soil is one of the most important parameters in hydrological models. However, owing to the lack of field data, hydraulic conductivity is frequently treated as a fitting parameter in the model to match the simulated and observed hydrographs (Whitaker et al. 2003). The lack of field data is particularly notable in sparsely populated mountainous and northern regions of Canada, where accessibility to watersheds is limited. There is a need for simple field methods using portable instruments to measure hydraulic conductivity in remote watersheds.

Constant-head well permeameter tests are commonly used to measure the field-saturated hydraulic conductivity of the soil around a well augered into the unsaturated zone (Reynolds and Elrick 2002). The Guelph permeameter (GP) is a portable device for conducting constant-head well permeameter tests using the Mariotte principle (Reynolds et al. 1985). The compactness of the GP makes it a potentially useful tool for measuring hydraulic conductivity in areas inaccessible by motorized vehicles. However, the standard GP data interpretation assumes that the soil is homogeneous and has an infinite extent. This condition is not met in soils whose physical properties vary with depth, or soils overlying an impermeable layer, such as bedrock, dense clay or permafrost. Soils of this type occupy large portions of the arctic and alpine tundra (National Research Council of Canada 1988), as well as the northern boreal forest (Quinton et al. 2003). Despite this limitation the GP is used in forest hydrology studies without carefully examining the effects of deviating from the assumptions (Sherlock et al. 2000).

Abbreviations: **GP**, Guelph permeameter

Laboratory permeameters offer an alternative method to determine the hydraulic conductivity of soil core samples, providing the samples are carefully collected so that the field conditions are preserved. This method is attractive for soils with a high degree of layering because each layer can be sampled separately. However, a large number of samples are required for proper representation of conductivity because the scale of such measurements is much smaller than that of field-based measurements. The laboratory core permeameter also has a potentially major problem for coarse-textured organic soil, where the leakage between the soil sample and the inner wall of the sample container can be substantial (Beckwith et al. 2003). Considering the prevalence of organic-covered terrain in northern and mountainous environments, it is desirable to use field methods, such as the GP, to obtain representative values of field-saturated hydraulic conductivity.

The objectives of this study were to: (1) examine the applicability of GP theory for soil overlying an impermeable substrate, (2) develop new data interpretation methods where the existing theory is not applicable, and (3) evaluate the effects of heterogeneity and anisotropy on the measured field-saturated hydraulic conductivity. A numerical simulation model was used for theoretical development. The new methods were tested in the laboratory and applied at a remote field site in the Northwest Territories, Canada

THEORY

Saturated-unsaturated flow around a well with a constant ponded head of water is described by Richards' equation expressed in cylindrical polar coordinates

$$\frac{1}{r}\frac{\partial}{\partial r}\left(rK(\psi)\frac{\partial h}{\partial r}\right)+\frac{\partial}{\partial z}\left(K(\psi)\frac{\partial h}{\partial z}\right)=C_w(\psi)\frac{\partial h}{\partial t} \quad (1)$$

where r [L] is radial distance, z [L] is elevation, t [T] is time, h [L] is total potential head, ψ [L] is matric potential head, K [L T^{-1}] is hydraulic conductivity, and C_w [L^{-1}] is specific water capacity. Based on the analytical and numerical solutions of Eq. 1, Elrick and Reynolds (1992) proposed a formula to estimate field-saturated hydraulic conductivity K_s [L T^{-1}] from the steady-state flow rate Q_s [L^3 T^{-1}]

$$K_s = Q_s\left(\frac{2\pi H^2}{C}+\frac{2\pi H}{\alpha^* C}+\pi a^2\right)^{-1} \quad (2)$$

where C is a dimensionless shape factor, α^* [L^{-1}] is a parameter representing the effects of soil capillarity under steady flow conditions, a [L] is the radius of the well, and H [L] is the steady depth of water in the well (see Fig. 1). Note that α^* is considered the integral equivalent (Reynolds and Elrick 1987) of α_G [L^{-1}] in Gardner's (1958) conductivity function. If an approximate value of α^* is known from soil texture and structure, the shape factor may be calculated from H/a (Reynolds and Elrick 1987). Equation 2 assumes homogeneous soil having an infinite extent. Reynolds and Elrick (1987) found that the flow around the well is unaffected by the boundaries if the boundaries are located at a distance of $10H$ from the well, implying that Eq. 2 may be used to interpret test results if the soil is homogeneous and the depth S [L] to the impermeable layer is sufficiently large.

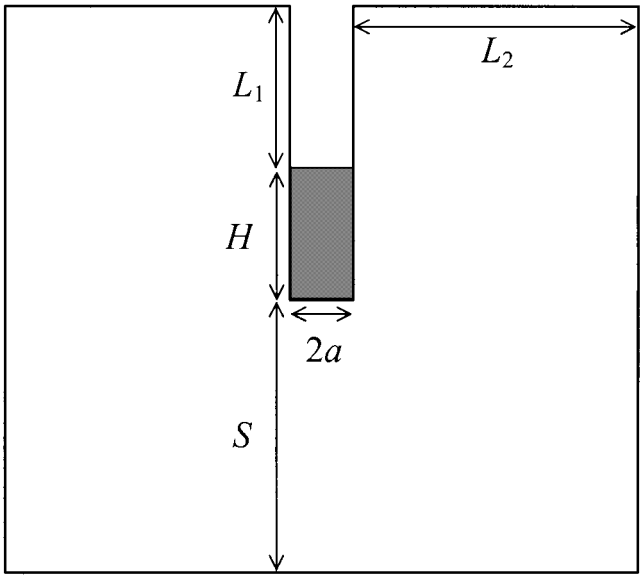

Fig. 1. Schematic diagram of the auger hole and the simulation domain. The shaded area indicates a steady ponded head of water.

METHODS

Numerical Simulation

The numerical model used in the present study is a modified version of Princeton UNSAT2D, which uses a mass-conservative finite element method to solve Richards' equation (Celia et al. 1990). The modification included an option to solve the cylindrical form of Richard's equation (Eq. 1) so that the three-dimensional flow can be simulated assuming the radial symmetry. The soil-water characteristics are represented by the van Genuchten (1980) equations

$$\Theta = [1 + (-\alpha\psi)^n]^{-m} \quad (3)$$

$$K = K_s\,\Theta^{1/2}\,[1-(1-\Theta^{1/m})^m]^2 \quad (4)$$

where

$$\Theta = (\theta - \theta_r)/(\theta_s - \theta_r) \quad (5)$$

$$m = 1 - 1/n \quad (6)$$

Θ is normalized volumetric soil water content defined by water content θ, water content at saturation θ_s, and residual water content θ_r remaining even at high soil tension, which is commonly treated as a fitting parameter. The dimensionless constant n represents the degree of sorting of soil particles and α [L^{-1}] is related to the reciprocal of air-entry matric potential head on the soil water retention curve. Small grid spacing ($\Delta r = 0.04a$ and $\Delta z = 0.2a$) was used in

the critical region around the auger hole to ensure the stability and accuracy of the solution, while larger spacing was used in the regions distant from the auger hole. The model was first validated by obtaining the steady-state numerical solutions of the Richards' equation using the same geometry and boundary conditions as those of Reynolds and Elrick (1987, Fig. 1), i.e., the auger hole placed in the centre of a cylinder, no-flow top and bottom boundaries, and constant-head outer boundary at the cylinder wall. The values of C calculated from numerical solutions in the present study (C_{PS}) were compared to those reported by Reynolds and Elrick (1987, Fig. 6) (C_{RE}), which were read on the graph using a ruler to an accuracy of ±0.2. The values were very close to each other (Table 1) and, therefore, the numerical model was validated for the present purposes. After the validation, the top and bottom boundaries were changed from constant head to no flow, and it was confirmed that the changes had no effects on C. The boundaries were then adjusted to reduce the size of the domain and the number of nodes, and hence computational time. It was found that the top boundary had negligible effects if $L_1/H > 1$ (see Fig. 1), and that the outer boundary had negligible effects if $L_2/H >$ 6.7 (see Fig. 1). The effects of the bottom boundary will be investigated below.

Laboratory Methods

Homogeneous, well-sorted sand with a mean particle diameter of 0.0041 m was packed to an approximate dry bulk density of 1700–1800 kg m^{-3} in a roughly cylindrical plastic tub having a radius of 0.22 m. The sand layer had a thickness of 0.2 m. Evenly spaced (0.05-m) holes with a diameter of 0.011m were made along the sidewall of the tub near the bottom to allow the lateral drainage of water. The K_s was measured using a core permeameter for six samples packed to approximately the same density as the sand in the tub. The samples were saturated from the bottom using tap water that had been equilibrated to room temperature but not deaired. Therefore, the condition was expected to be similar to the field-saturated condition with a small amount of entrapped air. Field-saturated hydraulic conductivity is generally smaller than the hydraulic conductivity of truly saturated soil without entrapped air (Reynolds et al. 1983). Mean and standard deviation of K_s for the six samples were $1.3 \pm 0.8 \times 10^{-4}$ m s^{-1}.

Porosity was estimated for six core samples from the measured dry bulk density and an estimate of particle density (Flint and Flint 2002). Mean porosity and standard deviation of the six samples was 0.35 ± 0.01 for a particle density of 2650 kg m^{-3} and 0.38 ± 0.01 for a particle density of 2800 kg m^{-3}. Actual soil particle density was not determined, but is expected to be between the two values. The soil water retention characteristic of the sand was measured on two samples having a diameter of 0.051 m and length of 0.050 m using the pressure extractor method (Dane and Hopmans 2002), and the van Genuchten function (Eq. 3) was fitted to the measured values using the least-squares method (Fig. 2). A well made of perforated PVC pipe with an outer diameter of 0.025 m was placed at the centre before the sand was packed. The bottom of the pipe was at the bottom of the tub. A tensiometer was installed at 0.14 m from the centre of the well to examine the soil moisture condition during tests. Constant-head tests were conducted in the sand using a Mariotte system similar to the GP.

Table 1. Comparison of C determined by numerical simulations in the present study (C_{PS}) and Reynolds and Elrick (1987, Fig. 6) (C_{RE})

α^* (m^{-1})	H/a	C_{PS}	C_{RE}
3.4	4	1.39	1.4
	8	2.03	2.1
25	4	1.49	1.5
	8	2.21	2.2

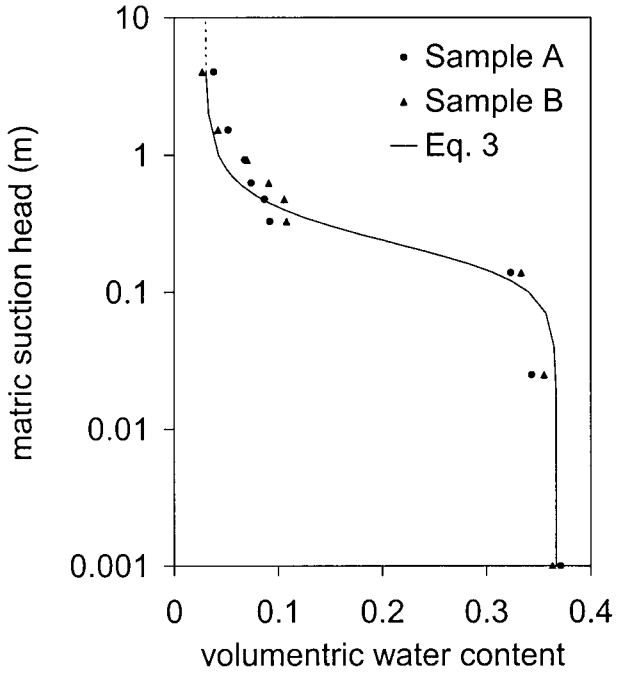

Fig. 2. Soil water retention characteristics for two samples of the sand. The solid curve shows Eq. 3 with $n = 3.0$, $\alpha = 5.1$ m^{-1}, $\theta_s = 0.37$, and $\theta_r = 0.03$.

RESULTS AND DISCUSSION

Effects of Impermeable Layer on the Shape Factor

Numerical simulations were conducted in model domains having various S/H ratios (see Fig. 1) to determine when the bottom boundary effects become important. Two cases of H/a (4 and 12) and two different types of soils were examined. The van Genuchten parameters (Eq. 3) of the two soils were common for n (= 1.5) but different for α (= 2.7 and 10 m^{-1}). The values of θ_s and θ_r would affect the transient part of simulations, but do not affect the steady-state flow rate at the end of the simulations. The boundary effect is most conveniently demonstrated using the shape factor C, calculated from Q and K_s (Eq. 2). Any deviation of C from C_∞ calculated for the sufficiently large simulation domain ($S/H = 20$) indicates the influence of the bottom boundary.

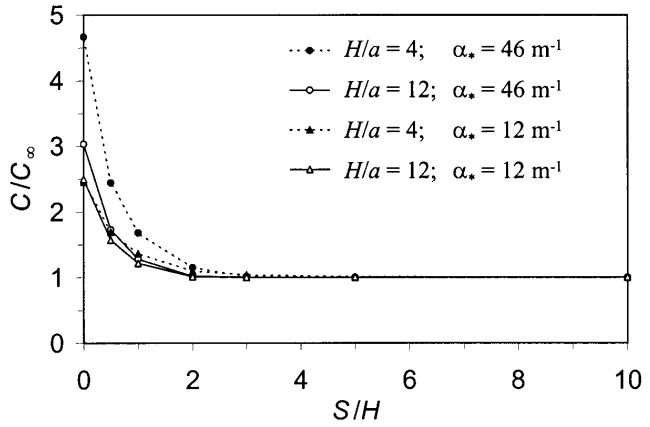

Fig. 3. Effects of changing *S*/*H* on *C* for the cases with *H*/*a* = 4 and 12.

The boundary effect was relatively minor (< 4 %) for both soils for *S*/*H* > 2 when *H*/*a* = 4, and for *S*/*H* > 1 when *H*/*a* = 12 (Fig. 3). Therefore, the standard method of analysis may be used to interpret the GP data even for the case with an impermeable layer if *S*/*H* is greater than 2. This is consistent with the recommendation by previous workers (Bouwer and Jackson 1974; Talsma and Hallam 1980).

Significant boundary effects were observed (Fig. 3) for smaller values of *S*/*H* and the effects were dependent on the soil type and *H*/*a*. Attempts were made to derive a "correction" factor for *C* to compensate for the boundary effect, but the correction factor was sensitive to the values of soil parameters (α and *n*) as well as *H*/*a*. Therefore, when the impermeable layer occurs at a relatively shallow depth, it is recommended to auger down to the impermeable layer so that the test is conducted with *S*/*H* = 0 to simplify the data analysis.

Time to Steady State

It is commonly assumed, based on the observation of flow rate, that "quasi-steady" state is achieved at less than 20–30 min after the commencement of the test (Talsma and Hallam 1980; Reynolds et al. 1983). The shape factor *C* in Eq. 2 is derived from the steady-state solutions of Richards' equation. Therefore, failing to achieve steady state during a test may result in misinterpretation of data. This issue is particularly important for the case with *S*/*H* = 0, where the flow around the auger hole is predominantly horizontal, which has more of the characteristics of two-dimensional than three-dimensional flow. For infiltration driven strictly by the pressure gradient, Philip (1969) found that steady state is achieved within a finite time for three-dimensional systems but never achieved for two- and one-dimensional systems. Therefore, it is expected that the time to quasi-steady state increases as *S*/*H* approaches zero.

Comparison between different flow configurations is most effectively presented using dimensionless variables Q^* and t^* (see Appendix for derivation).

$$Q^* = (Q - \pi a^2 K_s)/[2\pi K_s H(H + \alpha^{*-1})] \quad (7)$$

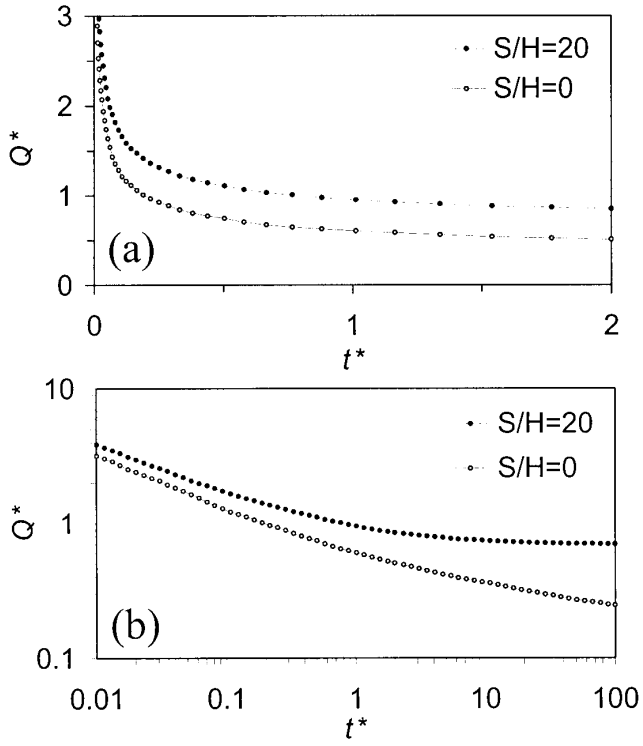

Fig. 4. Change in dimensionless flow rate Q^* with dimensionless time t^* for the case with *H*/*a* = 4, α = 10 m^{-1}, and *n* = 1.5. Two graphs show the identical data, but different scale for t^*.

$$t^* = tK_s / [a(\theta_s - \theta_i)] \quad (8)$$

where θ_i is the initial volumetric water content of the soil adjacent to the auger hole. Numerical simulations were conducted for various combinations of *H*/*a* and soil parameters (α and *n*) to evaluate the influence of varying *S*/*H* on the time to steady state. The effects of K_s and the moisture deficit $\theta_s - \theta_i$ do not have to be examined explicitly because dimensionless variables are used in this analysis.

Figure 4 shows an example for the case with *H*/*a* = 4, α = 10 m^{-1}, and *n* = 1.5. Visually inspecting Fig. 4a with t^* presented on the arithmetic scale, one may suggest that quasi-steady state is achieved at t^* = 1 for both unrestricted flow case (*S*/*H* = 20) and the case with the flow restricted by the impermeable layer (*S*/*H* = 0). However, the same data presented on logarithmic scales (Fig. 4b) show that for the restricted-flow case Q^* at t^* = 1 is significantly higher than the final value. Similar results were obtained for other combinations of *H*/*a* and soil parameters. In general quasi-steady state is achieved by t^* = 1 for unrestricted cases. In contrast Q^* keeps decreasing even after t^* = 10 for restricted cases, suggesting that some difficulty may be encountered in field tests. For example, consider a test conducted in a hole with *a* = 0.025 m for a soil having $K_s = 10^{-5}$ m s^{-1}, θ_s = 0.5, and θ_i = 0.2, representing typical values for soils in vegetated watersheds. In this case t^* = 1 corresponds to *t* = 750 s, which is consistent with the time to steady state reported by previous workers for unrestricted flow cases (< 1200–1800 s).

If the same test is conducted for the same soil, but with the flow restricted by an impermeable layer, steady state will not be achieved even after 7500 s or 2 h.

The values of C listed in Fig. 3 were calculated from Q^* when steady state was reached at $t^* = 10^4$ or greater. Therefore, strictly speaking, C can be used to interpret field data only under steady state conditions. However, it is clearly impractical to conduct field tests for hours or days to achieve steady state. Compared to the steady-state analysis, transient data analysis is much more susceptible to errors resulting from uncertainty in soil water retention characteristics. Therefore, it is necessary to set a practical value of t^* representing a quasi-steady state by examining the $Q^* - t^*$ curves of numerous cases covering a wide range of soil conditions.

Data Analysis for $S/H = 0$

Numerical simulations with $S/H = 0$ were conducted for 96 different combinations of variables; H/a = 2, 4, 8, 12; α = 5, 10, 30 m^{-1}; n = 1.3, 1.5, 2.0; and ψ_b = 0, –2, –10 m, where ψ_b is the initial matric potential head at the bottom boundary. Figure 5 shows an example of $Q^* - t^*$ curves for six simulations with varying H/a and α. Other simulations had similar curves. Upon inspecting these and other curves, it is proposed that $t^* = 3$ represents a quasi-steady state and that simulated value of Q at $t^* = 3$ is regarded as the quasi-steady-state flow rate (Q_s) in Eq. 2. The rational is: (1) $t^* = 3$ corresponds to reasonable time (< 1 h) for most natural soils in vegetated watersheds, (2) the rate of change in Q with time is slow after $t^* = 3$, for example Q at $t^* = 6$ is only 10–20 % lower than Q at $t^* = 3$ for all cases, and (3) Q_s can be used with the method described below that is operationally identical to the standard GP data analysis.

To calculate K_s from Q_s using Eq. 2, the shape factor C needs to be evaluated for various H/a and soil parameters. The standard GP data interpretation assumes that C can be estimated accurately from H/a and α^* because steady-state flow in homogeneous, infinite soil is completely characterized by K_s, H/a, and α^*. The validity of this assumption for the restricted-flow case will be examined below. For all tested combinations of (α, n, ψ_b), C increased with α^* and H/a (Fig. 6). This is similar to the relation between C and H/a for unrestricted cases (Reynolds and Elrick 2002). Despite some scatter it is possible to define $C - \alpha^*$ curves corresponding to specified values of H/a:

$$C = u - s \exp(- p\, \alpha^*) \tag{9}$$

where u, s, and p [L] are coefficients dependent on H/a by the following relation.

$$p = p_1 (H/a)^{p2} \tag{9a}$$

$$s = s_1 + s_2 \exp(- s_3\, H/a) \tag{9b}$$

$$u = u_1 + u_2\, H/a \tag{9c}$$

where p_1 [L], p_2, s_1, s_2, s_3, u_1, and u_2 are fitting parameters. The $C - \alpha^*$ curves corresponding to each H/a value were almost identical between simulations with moderately dry initial and boundary conditions, ψ_b = –2 m (Fig. 6a) and very dry conditions, ψ_b = –10 m (not shown). However, the curves were noticeably different for simulations with very wet conditions, ψ_b = 0 (Fig. 6b). Therefore, a set of parameter values corresponding to dry conditions (Table 2) was determined by fitting all parameters in Eqs. 9a–c simultaneously to all data points in Fig. 6a using the least-squares method. Similarly another set of parameters values corresponding to wet conditions (Table 2) was determined for the data points in Fig. 6b.

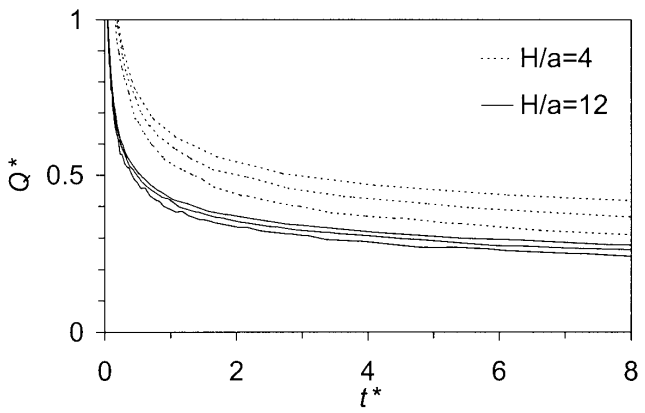

Fig. 5. $Q^* - t^*$ curves for the cases with n = 1.5 and ψ_b = –2 m. Three curves with varying α are shown for each of the two H/a. The top curve is for α = 5 m^{-1}, the middle for α = 10 m^{-1}, and the bottom for α = 30 m^{-1}.

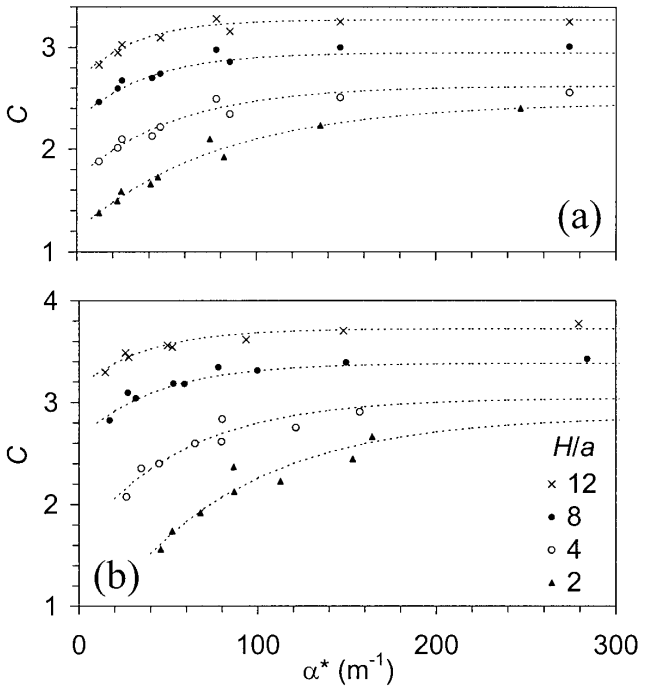

Fig. 6. Relation between C and α^* for selected values of H/a. (a) Dry conditions represented by ψ_b = –2 m. (b) Wet conditions represented by ψ_b = 0. Curves show Eq. 9 with the coefficients determined by the least-squares method.

Table 2 Parameter values for Eq. 9

	p_1	p_2	s_1	s_2	s_3	u_1	u_2
Dry ($\psi_b \leq -2$ m)	0.00862	0.532	0.607	1.40	0.380	2.30	0.0813
Wet ($\psi_b \cong 0$)	0.00999	0.398	0.530	3.61	0.357	2.71	0.0848

Previously published values of C for the homogeneous, infinite soil are lower than the values given by Eq. 9 (Fig. 7). Therefore, using previously published C values for soils underlain by an impermeable boundary will result in the underestimation of K_s, although the difference may be relatively small compared to other uncertainties including measurement errors, estimate of α^*, and soil heterogeneity.

To apply the new shape factor, an approximate time corresponding to $t^* = 3$ should be estimated first from available information. This will aid in planning the test, for example estimating the expected test duration and the required amount of water. An approximate value of α^* also needs to be estimated from the soil textural and structural type (Reynolds et al. 2002, Table 3.4–4). The flow rate should be monitored during the test until a reasonably constant value of Q, taken to be Q_s, is reached. After K_s is calculated from Q_s using Eq. 2, the value of t^* at the end of the test should be recalculated to verify that it is reasonably close to 3.

Validation of the Method by Laboratory Tests

The laboratory sand had an average K_s of $1.3 \pm 0.8 \times 10^{-4}$ m s^{-1} and θ_s of 0.37 ± 0.01 (variability estimated from that of porosity). The radius of the well (a) was 0.0125 m, and the sand was initially dry ($\theta_i \cong 0$). Therefore, $t^* = 3$ corresponds to $t = 107$ s according to Eq. 8. A constant-head test was conducted with $H = 0.065$ m. The flow rate quickly reached stable values (Fig. 8) although the values fluctuated randomly due to the limited accuracy of manually reading the scale on the water reservoir. After about 700 s the flow rate decreased due to the boundary effects of the container wall. The tensiometer located 0.08 m from the boundary started to respond at 600 s and reached near zero tension by 800 s.

The average flow rate during the steady period between 100 and 400 s was 6.0 mL s^{-1} (Fig. 8). The α^* calculated from numerically integrating the water retention function (Fig. 2) was 8.5 m^{-1}. Using Eq. 9 with the set of parameters for the dry conditions (Table 2), C is estimated to be 2.05 for $H/a = 5.2$. Substituting $Q_s = 6.0 \times 10^{-6}$ m^3 s^{-1} and $\alpha^* = 8.5$ m^{-1} and $C = 2.05$ into Eq. 2 gives $K_s = 1.6 \times 10^{-4}$ m s^{-1}. This is within the range of K_s (= $1.3 \pm 0.8 \times 10^{-4}$ m s^{-1}) determined by core permeameter tests, which is expected to represent the field-saturated condition. Another test was conducted on a separate sand tank having the identical construction, but with $H = 0.05$ m. The average Q during the steady period was 3.3 mL s^{-1}, which gave $K_s = 1.1 \times 10^{-4}$ m s^{-1}. Therefore, the proposed method using Eq. 2 and Fig. 6 (or Eq. 9) is expected to give reliable results for relatively homogeneous and isotropic soils.

Effects of Anisotropy and Heterogeneity

Anisotropic soil has a horizontal saturated hydraulic conductivity (K_{sH}) significantly different from the vertical conductivity (K_{sV}). A set of numerical simulations with $K_{sH}/K_{sV} = 0.1$, 1, and 10 was conducted for various combination of H, α, and n to examine the effects of anisotropy with an impermeable bottom boundary. The flow rate at $t^* = 3$ was nearly identical between the cases with $K_{sH}/K_{sV} = 0.1$, 1, and 10, suggesting that the anisotropy effect is negligible and that the K_s determined by the GP method represents horizontal hydraulic conductivity. This is presumably because the flow direction is mainly horizontal as shown by numerically simulated flow lines around the auger hole (Fig. 9). It should be noted that when auger hole tests, such as the GP method, are applied under unrestricted flow condition, they generally measure the combined effects of K_{sH} and K_{sV} (Hyder and Butler 1995). The predominantly horizontal flow in the present numerical simulation is forced by the impermeable bottom boundary.

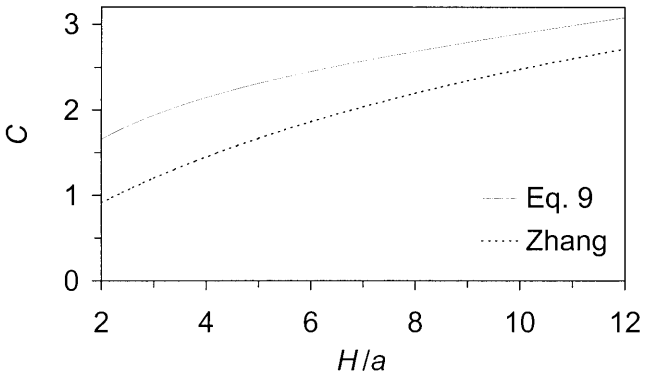

Fig. 7. Comparison of C values calculated using Eq. 9 and Zhang et al. (1998, Eq. 1) for sands ($\alpha^* = 36$ m^{-1}). Parameters for dry conditions (Table 2) are used in Eq. 9.

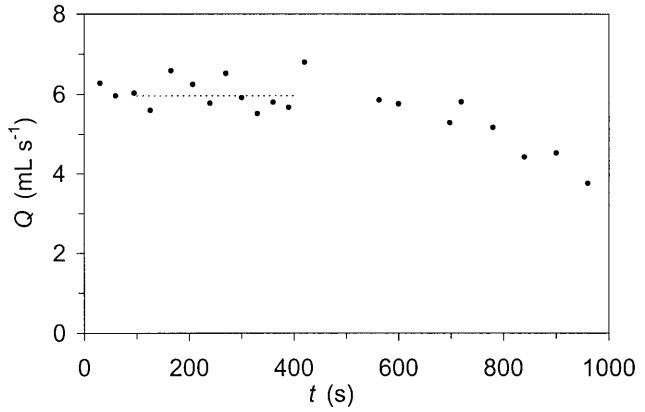

Fig. 8. Flow rates during a sand-tank test. The dashed line indicates the average flow rate between $t = 100$ and 400 s.

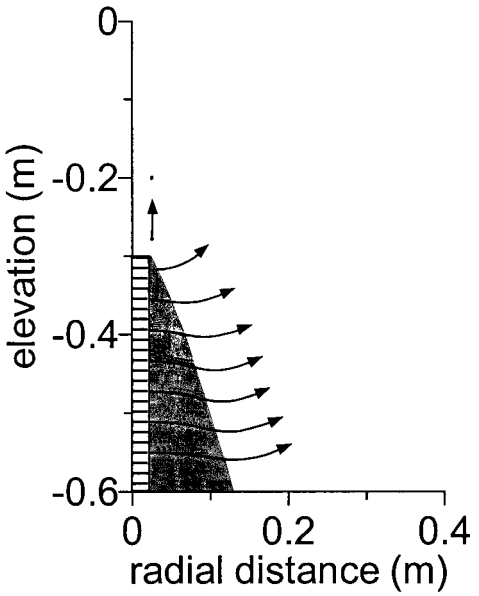

Fig. 9. Flow pattern around the auger hole (H = 0.3 m, a = 0.025 m) for isotropic soil with parameters $\alpha = 5\ m^{-1}$, n = 1.5, and ψ_b = –2 m. The shaded area indicates the zone of saturation and solid lines indicate the trajectory of particles released from the well. The line length roughly represents the travel distance at t^* = 3 of imaginary particles released from the dots. Note that flow velocity is negligible at an elevation of –0.2 m.

Natural soil is generally heterogeneous. In particular layered heterogeneity is commonly observed in forest soil, where hydraulic conductivity decreases with depth (Talsma and Hallam 1980). The GP method measures the bulk K_s of the soil around the auger hole in a weighted-average sense, where individual soil layes have different weights. It is impossible to determine a priori the exact weighting function in heterogeneous soil, but the relative importance of individual layers can be represented by a filter function G similar to Beckie (2001).

$$\delta K_s = G\delta k_s \tag{12}$$

where δK_s is the change in "measured" bulk saturated conductivity and δk_s is the change in the saturated conductivity of an individual layer. Figure 10a shows an example of the filter function determined by a series of numerical simulations. A change in one unit of conductivity for the 0.05-m-thick bottom layer changes the measured bulk conductivity by 0.143 units. The filter function is greater near the bottom and is negligible above the water level in the auger hole (–0.3 m in Fig. 10a), indicating that the GP method measures the conductivity of the saturated region and that the measured K_s is more sensitive to the lower layers.

The depth-variation of the filter function is related to the variation of horizontal Darcy flux along the auger hole (Fig. 10b), which decreases upwards. The radius of the saturated region is greatest near the bottom of the hole (Fig. 9) offering relatively low flow resistance. The measured bulk conductivity is most sensitive to the change in the conductivity of the high flow zone at the bottom.

Field Example

An application of the new data analysis method is demonstrated by a field test conducted at the Scotty Creek watershed located approximately 60-km south of Fort Simpson, Northwest Territories (Quinton et al. 2003). The study site is accessible only by a helicopter, requiring the instrument to be as small and light as possible. The site is situated on a peat plateau (Robinson and Moore` 2000) and represents a typical organic terrain of the wetland-dominated, northern boreal region in the zone of discontinuous permafrost. Shrubs and black spruce (*Picea marinara*) grow through the ground cover composed of lichens and mosses overlying sylvic peat having an estimated thickness of 3–4 m. The peat was nearly saturated and frozen to the ground surface during winter, and thawed and drained down to a depth of 0.5 m when the test was conducted 2001 Aug. 26. The top surface of frozen peat, or the frost table, was considered an impermeable boundary because saturated frozen peat has very low permeability (Roulet and Woo 1986).

The unfrozen peat had fairly high hydraulic conductivity and it was deemed impractical to use the Mariotte system of the GP to maintain the constant head and measure flow rates throughout the test. Therefore, constant head was maintained by manually pouring water into the well while monitoring the water level with an electronic sounder and keeping track of the amount of water poured. The water-filled Mariotte system was initially placed in the well with the reservoir valve closed. At t = 20 min, the valve was opened and the flow rate was accurately measured using the Mariotte system until the inner reservoir was empty. After this measurement the manual measurement started while the reservoir was filled with water for the next measurement. The flow rate was measured in this manner three times during the test; Q = 0.64 mL s^{-1} at t = 20 min, 0.63 mL s^{-1} at 27 min, and 0.59 mL s^{-1} at 50 min. The bottom of the hole was at the frost table (S = 0) and the test was conducted with H = 0.10 m and a = 0.025 m.

The van Genuchten parameters were determined by fitting a curve to the water retention characteristic of an undisturbed sample of peat at 0.40-m depth measured by the pressure extractor method; n = 1.4, $\alpha = 4\ m^{-1}$, θ_s = 0.8, and θ_r = 0.25. The peat was fairly moist with an estimated pressure head of –0.1 m. The α^* calculated from integrating the van Genuchten function is 35 m^{-1} and, hence, Eq. 9 gives C = 2.14 using the "wet" values of fitting parameters in Table 2. Using Q_s = 0.6 mL s^{-1} in Eq. 2 gives $K_s = 1.5 \times 10^{-5}$ m s^{-1}. Assuming θ_i = 0.5, the value of t^* at t = 50 min is 6.4 (Eq. 8) indicating that quasi-steady state was reached during the test.

When the van Genuchten parameters are not available, as in most field studies, α^* needs to be estimated from soil texture and structural categories (Reynolds et al. 2002). In this example, estimating $\alpha^* = 10\ m^{-1}$ would have given $K_s = 1.0 \times 10^{-5}$ m s^{-1} and $\alpha^* = 100\ m^{-1}$ would have given $K_s = 1.8 \times 10^{-5}$ m s^{-1}. Therefore, the errors in K_s resulting from the errors in α^* are relatively small. Our analysis of water retention characteristics of other peat samples from several sites in northern

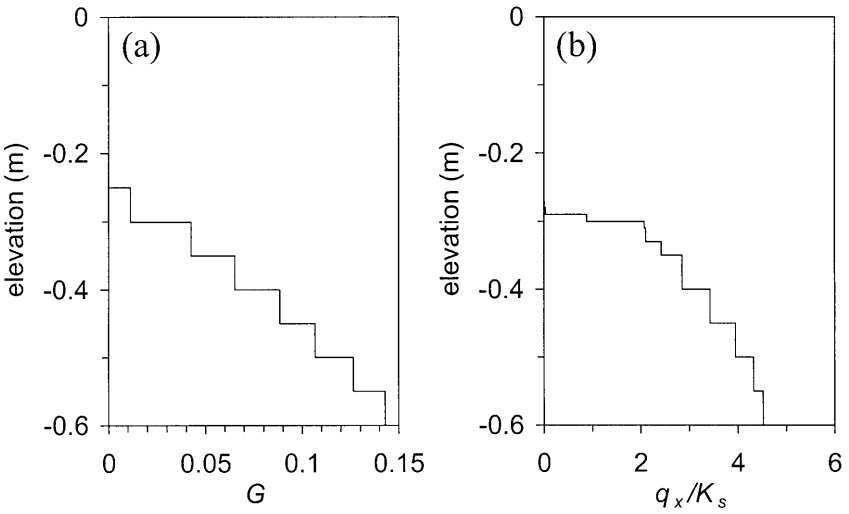

Fig. 10. (a) Distribution of the conductivity weighting function (G) for the case with H = 0.3 m, α = 5 m^{-1}, n = 1.5, and ψ_b = –2 m. (b) Distribution of the horizontal component of Darcy flux (q_x) for the same case.

Canada suggest that α^* = 40 m^{-1} is appropriate for decomposed peat and 100 m^{-1} is appropriate for relatively undecomposed peat.

CONCLUSIONS

The influence of an impermeable layer on constant-head well permeameter tests, the Guelph Permeameter (GP) in particular, was examined using numerical simulations. The existing published values of the shape factor, C can be used to interpret the data when the distance S between the impermeable layer and the bottom of the auger hole is sufficiently large ($S/H > 2$). However, this method may significantly underestimate hydraulic conductivity when the distance is too small. In such a case, it is recommended to auger the hole down to the impermeable layer so that $S = 0$ and use a new set of C values to analyze the data. The flow around the auger hole is predominantly horizontal, i.e., two dimensional, when it is restricted by the impermeable layer. Therefore, it requires more time to reach steady state compared to the cases with unrestricted three-dimensional flow. The new values of C for the restricted flow cases were determined for a "quasi-steady" state condition. The GP method measures horizontal hydraulic conductivity because anisotropy has insignificant effects when the flow is mainly horizontal. The measured conductivity represents a weighted average conductivity of the soil surrounding the wet part of the auger hole. In soils with depth-varying conductivity, the weight is higher on the zones close to the bottom of the hole than those close to the top.

ACKNOWLEDGEMENT

We thank Michael Toews for skillfully running a large number of simulations and Joshua Brown for carrying out laboratory experiments. The source code of Princeton UNSAT2D was provided by the courtesy of Michael Celia. Constructive comments by the two anonymous reviewers greatly improved the manuscript. This study was funded by the Canadian Foundation for Climate and Atmospheric Science, Natural Sciences and Engineering Research Council, and Environment Canada Science Horizons Program.

Beckie, R. 2001. A comparison of methods to determine measurement support volumes. Water Resour. Res. **37**: 925–936.

Beckwith, C. W., Baird, A. J. and Heathwaite, A. L. 2003. Anisotropy and depth-related heterogeneity of hydraulic conductivity in a bog peat. I. Laboratory measurements. Hydrol. Processes **17**: 89–101.

Bouwer, H. and Jackson, R. D. 1974. Determining soil properties. Pages 611–666 *in* J. van Schilfgaarde, ed. Drainage for agriculture. Agronomy 17. ASA, Madison, WI.

Celia, M. A., Bouloutas, E. T. and Zarba, R. L. 1990. A general mass-conservative numerical solution for the unsaturated flow equation. Water Resour. Res. **26**: 1483–1496.

Dane, J. H. and Hopmans, J. W. 2002. Pressure plate extractor. Pages 688–690 *in* J. H. Dane and G. C. Topp, eds. Methods of soil analysis. Part 4. Physical methods. SSSA Book Series 5, Madison, WI.

Elrick, D. E. and Reynolds, W. D. 1992. Methods for analyzing constant-head well permeameter data. Soil Sci. Soc. Am. J. **56**: 320–323.

Flint, A. L. and Flint, L. E. 2002. Porosity. Pages 241–254 *in* J. H. Dane and G. C. Topp, eds. Methods of soil analysis. Part 4. Physical methods. SSSA Book Series 5, Madison, WI.

Gardner, W. R. 1958. Some steady-state solutions of the unsaturated moisture flow equation with application to evaporation from a water table. Soil Sci. **58**: 228–232.

Hyder, Z. and Butler, J. J. 1995. Slug tests in unconfined formations: An assessment of the Bouwer and Rice technique. Ground Water **33**: 16–22.

National Research Council of Canada. 1988. Glossary of permafrost and related ground-ice terms, Permafrost Subcommittee, Associate Committee on Geotechnical Research. Technical Memorandum No. 142, Ottawa, ON.

Philip, J. R. 1969. Absorption and infiltration in two- and three-dimensional systems. Pages 503–525 *in* R. E. Rijtema and H. Wassink, eds. Water in the unsaturated zone. 1966, Vol. 1. Proceedings of ASH/UNESCO Symposium, Wageningen, The Netherlands.

Quinton, W. L., Hayashi, M. and Pietroniro, A. 2003. Connectivity and storage functions of channel fens and flat bogs in northern basins. Hydrol. Processes **17**: 3665–3684.

Reynolds, W. D. and Elrick, D. E. 1987. A laboratory and numerical assessment of the Guelph permeameter method. Soil Sci. **144**: 282–299.

Reynolds, W. D. and Elrick, D. E. 2002. Constant head well permeameter (vadose zone). Pages 844–858 *in* J. H. Dane and G. C. Topp, eds. Methods of soil analysis. Part 4. Physical methods. SSSA Book Series 5, Madison, WI.

Reynolds, W. D., Elrick, D. E. and Clothier, B. E. 1985. The constant head well permeameter: Effect of unsaturated flow. Soil Sci. **139**: 172–180.

Reynolds, W. D., Elrick, D. E. and Topp, G. C. 1983. A reexamination of the constant head well permeameter method for measuring saturated hydraulic conductivity above the water table. Soil Sci. **136**: 250–268.

Reynolds, W. D., Elrick, D. E. and Youngs, E. G. 2002. Ring or cylinder infiltrometers (vadose zone). Pages 818–820 *in* J. H. Dane and G. C. Topp, eds. Methods of soil analysis. Part 4. Physical methods. SSSA Book Series 5, Madison, WI.

Robinson S. D. and Moore, T. R. 2000. The influence of permafrost and fire upon carbon accumulation in high boreal peatlands, Northwest Territories, Canada. Arct. Antarct. Alp. Res. **32**: 155–166.

Roulet, N. T. and Woo, M.-K. 1986. Hydrology of a wetland in the continuous permafrost region. J. Hydrol. **89**: 73–91.

Sherlock, M. D., Chappell, N. A. and McDonnell, J. J. 2000. Effects of experimental uncertainty on the calculation of hillslope flow paths. Hydrol. Processes **14**: 2457–2471.

Talsma, T. and Hallam, P. M. 1980. Hydraulic conductivity measurement of forest catchments. Aust. J. Soil Res. **18**: 139–148.

van Genuchten, M. T. 1980. A closed-form equation for predicting the hydraulic conductivity of unsaturated soils. Soil Sci. Soc. Am. J. **44**: 892–898.

Whitaker, A., Alila, Y., Beckers, J. and Toews, D. 2003. Application of the distributed hydrology soil vegetation model to Redfish Creek, British Columbia: Model evaluation using internal catchment area. Hydrol. Proc. **17**: 199–224.

Zhang, Z. F., Groenevelt, P. H. and Parkin, G. W. 1998. The well-shape factor for the measurement of soil hydraulic properties using the Guelph Permeameter. Soil Tillage Res. **49**: 219–221.

APPENDIX

Notation

a	radius of the well [L]
$c(\psi^*)$	dimensionless water capacity
C	shape factor
C_∞	shape factor for very large S/H
$C_w(\psi)$	specific water capacity [L^{-1}]
G	filter function
h	total potential head [L]
H	height of water in the well [L]
$k(\psi^*)$	dimensionless relative conductivity
$K(\psi)$	hydraulic conductivity [LT^{-1}]
k_s	saturated hydraulic conductivity of individual layers [LT^{-1}]
K_s	saturated hydraulic conductivity [LT^{-1}]
K_{sH}	horizontal saturated hydraulic conductivity [LT^{-1}]
K_{sV}	vertical saturated hydraulic conductivity [LT^{-1}]
L_1	distance between the well and the top boundary [L]
L_2	distance between the well and the outer boundary [L]
m	van Genuchten parameter
n	van Genuchten parameter
p	fitting parameter [L]
p_1	fitting parameter [L]
p_2	fitting parameter
Q	flow rate out of the well [L^3T^{-1}]
Q^*	Dimensionless flow rate
Q_s	steady-state flow rate [L^3T^{-1}]
r	radial distance [L]
r_*	dimensionless radial distance
s	fitting parameter
s_1	fitting parameter
s_2	fitting parameter
s_3	fitting parameter
S	distance between the well and the bottom boundary [L]
t	time [T]
t^*	dimensionless time
u	fitting parameter
u_1	fitting parameter
u_2	fitting parameter
z	elevation [L]
z^*	dimensionless elevation
α	van Genuchten parameter [L^{-1}]
α_G	parameter for the Gardner conductivity function [L^{-1}]
α^*	integral equivalent of α_G [L^{-1}]
θ	volumetric water content
θ_i	initial water content
θ_r	residual water content
θ_s	saturated water content
Θ	normalized water content
τ	characteristic time [T]
ψ	matric potential head [L]
ψ_b	initial values of matric potential head at the bottom boundary [L]
ψ^*	dimensionless matric potential

Derivation of the Dimensionless Form of Richards Equation

We define dimensionless variables

$$r^* = r/a \qquad z^* = z/a \qquad \psi^* = \alpha\psi \qquad t^* = t/\tau \tag{A1}$$

where ψ [L] is matric potential head and τ [T] is the characteristic time defined by

$$\tau = a\,(\theta_s - \theta_i)/K_s \tag{A2}$$

Initial water content θ_i is the water content of the soil adjacent to the auger hole. We also note that van Genuchten functions may be expressed in terms of dimensionless relative hydraulic conductivity k and specific water capacity c as

$$k(\psi_*) = \frac{\left\{1 - |\psi_*|^{n-1}\left[1 + |\psi_*|^n\right]^{-m}\right\}^2}{\left[1 + |\psi_*|^n\right]^{m/2}} \tag{A3}$$

$$c(\psi_*) = \frac{nm|\psi_*|^{nm}}{\left[1 + |\psi_*|^n\right]^{1+m}} \tag{A4}$$

so that $K = kK_s$ and $C_w = c\alpha\,(\theta_s - \theta_i)$. Using the dimensionless variables and noting that

$$h = z + \psi \tag{A5}$$

where z axis is taken to be positive upwards, Eq. 1 may be written

$$\frac{1}{r_*}\frac{\partial}{\partial r_*}\left(r_* k \frac{\partial \psi_*}{\partial r_*}\right)+\frac{\partial}{\partial z_*}\left(k\frac{\partial \psi_*}{\partial z_*}\right)+a\alpha\frac{\partial k}{\partial z_*}=a\alpha c\frac{\partial \psi_*}{\partial t_*} \quad \text{(A6)}$$

It is necessary to represent the transient flow rate out of the auger hole Q [L^3 T^{-1}] as a dimensionless variable for the analysis of the time to steady state. We replace Q_s in Eq. 2 by Q and rearrange the equation so that

$$\frac{1}{C}=\frac{Q-\pi a^2 K_s}{2\pi K_s H\left(H+1/\alpha_*\right)} \quad \text{(A7)}$$

Noting that the numerator on the right-hand side represents pressure-driven flow rate and the denominator represents the driving force,

$$Q^* = 1/C \quad \text{(A8)}$$

defines the dimensionless flow rate Q^*.